Adhesive Strengths Between Glass Fiber-Filled ABS and Metal in Insert Molding With Engraved and Embossed Metal Surface Treatments

Se Lyn Kim, Min-Young Lyu

Department of Mechanical System Design Engineering, Seoul National University of Science and Technology, 232 Gongneung-ro, Nowon-gu, Seoul 01811, South Korea

Metal and plastic can be bonded in a single molding process by metal insert molding, in which a metal is inserted into a mold and a plastic resin is then injected. However, the adhesive strength at the interface between the metal and plastic is weakened by the difference in the shrinkage ratio and inherent differences between the materials in the metal insert molding. This study reports the treatment of a metal surface that is followed by inserting the metal into a mold to increase the adhesive strength between the metal and glass fiber (GF)-filled acrylonitrile butadiene styrene (ABS). A laser process was used for an engraving surface treatment and a plating process was performed for an embossed surface treatment of the metal. In addition, the adhesive strength between the metal and GF-filled ABS was evaluated after the insert molding process was completed. Particles such as glass beads, ceramic beads, artificial diamonds, and aluminum oxides were employed in the plating process. The adhesive strength varied depending on the surface treatment of the metal. In particular, the adhesive strength significantly increased when an undercut shape was formed at the metal surface. The best adhesive strength with GF-filled ABS was found in the metal specimen plated using aluminum oxide particles. POLYM. ENG. SCI., 59:E93–E100, 2019. © 2018 Society of Plastics Engineers

INTRODUCTION

Product design has evolved into emotional design because the design stimulates the user's emotion, which is in contrast to earlier design concepts that only focused on functional and manufacturing viewpoints [1, 2]. Since the exterior design of products is one of the factors that contribute most to a consumer's selection, it is necessary to search for new design directions according to the trends and reflect the new design trends in actual products. Plastic materials are mainly used for product exteriors. In addition, designs with a metallic effect have been used to give a stately feeling to light plastic materials [3, 4]. To give a metallic effect to plastic products, post-processing such as coating or plating after molding has generally been employed [5]. However, with added processing the manufacturing cost and defect rate tend to increase. To overcome this drawback, methods that implement the metallic effect on a plastic surface without post-processing have been proposed. One such method is injection molding that uses the so-called pearl resin, which is fabricated by adding aluminum flakes to the base resin. Another method is metal insert molding, in which metal and plastic are directly bonded in the injection molding process. Metal insert molding can use several types of metals and there is a high degree of freedom in design.

The proposed insert molding process is as follows. A metal piece processed to a desirable shape is inserted into the mold and molten plastic is injected over the metal, thereby bonding the metal and plastic materials in the mold [6–8]. The adhesion between the metal and plastic is very important in insert molding. We examined theoretical reviews for interfacial adhesive fracture in the literature [9, 10]. The cracking of glued interfaces is fractured when plastic flow occurs in the adherends. Mittal [11] stipulated the role of the interface in adherend–adherate combinations and examined the strength of adhesive joints. He revealed that the interfacial tension between the substrate and the adhesive was the most important factor for adhesive joint strength. Fourche [12] reviewed theoretical concepts and adhesion models between two substrates and explained their mechanism. We review three methods to improve adhesion [8, 13]. In the first method, the adhesive is applied to a metal surface before insert molding is performed. However, the adhesive may be degraded by the high temperature during injection molding or it may be washed out during molding, which limits the adhesive strength [14, 15]. The second method increases the surface energy of the metal, which is proportional to adhesive strength [14, 16, 17]. Shear stress occurs at the interface between the plastic and metal due to a difference in shrinkage ratio during cooling after the injected high-temperature plastic contacts the metal and adheres during the insert molding. This method suffers from a limitation in obtaining sufficient adhesive strength that can endure shear stress at the interface with only an increase in surface energy of the metal [18]. The third method increases the surface area to improve the adhesive strength between the metal and plastic, for which a sufficient adhesive area between the metal and plastic should be ensured by a process that roughens the metal surface [14]. However, even if the surface area is increased by the rough surface of the metal, the adhesive strength is not necessarily proportional to the surface area [19]. If the rose petal effect occurs, in which the plastic resin is not inserted into a roughly processed metal surface but floated over the surface, adhesion is not achieved [20, 21]. Thus, the size of grooves where resins flow well into the surface area of the metal needs to be adjusted, and simply increasing the surface area of the metal by the metal insert molding is not adequate. It is also important to make an undercut shape in the metal surface to prevent inserted plastic resins from getting away from the surface easily [22]. However, few systematic and scientific studies have been conducted on adhesion between the

Correspondence to: M.-Y. Lyu; e-mail: mylyu@seoultech.ac.kr
Contract grant sponsor: Ministry of Trade, Industry and Energy (MOTIE) of Korea; contract grant number: 10051680.
DOI 10.1002/pen.24866
Published online in Wiley Online Library (wileyonlinelibrary.com).

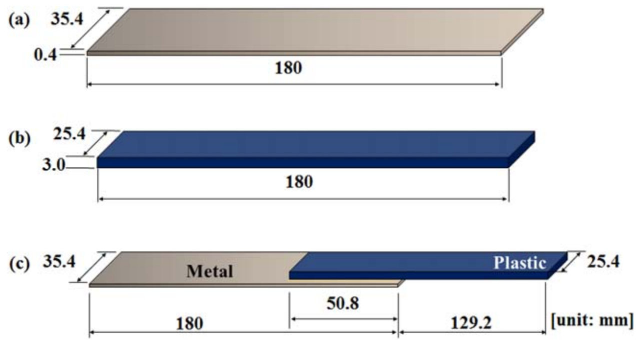

FIG. 1. Specimen for the metal-plastic adhesion test. (a) Metal part, (b) Plastic part, (c) Overall shape of insert molded specimen for the lab-shear test.

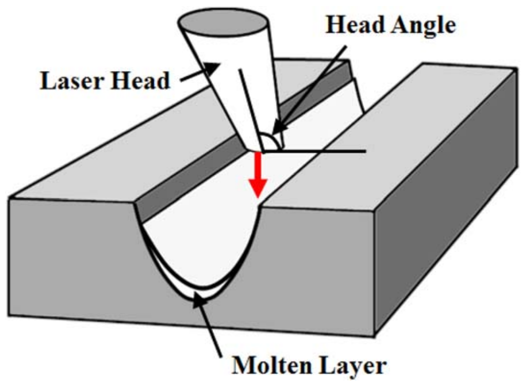

FIG. 2. Schematic drawing of laser machining process.

metal and plastic during the insert molding process and the application of insert molding to real products is also limited.

Thus, the aim of our study was to identify a method that improved adhesive strength between the metal and plastic during metal insert molding by controlling the metal surface morphology. To this end, in our study, the metal surface was processed by combining the widely used method of engraved surface processing with the embossed surface processing method. For engraving, laser processing was used to process the metal surface by controlling the laser head angle and processing pattern. Nickel electroplating with particles was employed for the embossed surface processing method. We investigated the effect of processing the metal surface on the adhesion between the metal and plastic by adjusting the type and size of particles.

EXPERIMENTAL

Materials

The plastic resin used in this study was acrylonitrile butadiene styrene (ABS) (STAREX GR-4030, Cheil Industries Inc.) containing 30 wt% glass fiber (GF). A 0.4-mm thick steel use stainless (SUS) sheet was used for the metal specimen.

Experiment Model

To measure the adhesive strength between the metal and plastic, specimens that met the ASTM D1002 standard were utilized. The shape of the metal and plastic for adhesion using insert molding is shown in Fig. 1a and b. The surface of the metal specimen shown in Fig. 1a was processed and the final insert molding specimen with plastic over the metal surface (Fig. 1b) is shown in Fig. 1c for the lab-shear test.

Metal Surface Treatment

Engraving Surface Processing. The engraving surface processing method was conducted using a laser to increase the surface area of the metal specimen. Laser processing is a method that uses a special light called a laser. It melts and processes a target object locally using thermal energy converted from light. A schematic diagram of laser processing is shown in Fig. 2. Laser processing that processes a target object locally is characterized by a low burden on the entire surface of the metal specimen and a facile increase in the processing depth. A metal specimen processed to about 100-μm depth using laser processing was fabricated. The metal specimen was fabricated by controlling the laser head angle and processing pattern. Table 1 presents the laser processing conditions used in this study. A right angle cross refers to processing along the perpendicularly crossed path shown in Fig. 3a to generate a rectangular mesh-shaped pattern on the metal surface. In the right angle cross condition, the laser head angle was set to 45° and 90° to fabricate the metal specimen. A parallel line refers to processing along a straight line as shown in Fig. 3b to make parallel stripes on the metal surface. The laser head angle was set to 45° and 135° alternately to fabricate a metal specimen with parallel lines. A diagonal cross refers to processing along the orthogonally crossed path as shown in Fig. 3c to generate a diamond shaped pattern on the metal surface. The laser head angle was set to 45° to fabricate a metal specimen with a diagonal cross.

Embossed Surface Processing. Nickel electroplating with particles was used. The plating process is as follows. Prior to plating, the metal specimen was immersed in a 45°C 1.3 wt% NaOH solution for 1 min followed by 20°C 35 wt% HCl solution for 1 min to remove impurities and oil from the metal surface. The SUS surface is highly stable so its adhesion with a nickel-plating layer is weak. Thus, if nickel plating is performed on the SUS surface immediately after impurities are removed, the nickel-plating layer may not undergo proper electrodeposition [23]. Hence, nickel chloride plating was conducted in a solution containing 2.4 wt% $NiCl_2$ and 1.25 wt% HCl prior to nickel plating. Afterward, the SUS surface was immersed in a solution containing 3 wt% $NiSO_4$, 5 wt% $NiCl_2$, and 0.5 wt% H_3BO_3; the particles were sprayed to conduct nickel plating. We took advantage of an electroplating process in which particles in the solution were mixed and plated on the base metal surface when the metal was precipitated. The particles that were sprayed over the metal surface inside the nickel plating bath attached to the metal surface while nickel was plated to the

TABLE 1. Laser machining conditions.

Machining path	Laser head angle
Right angle cross	45°
	90°
Parallel line	45°, 135°
Diagonal cross	45°

 DOI 10.1002/pen

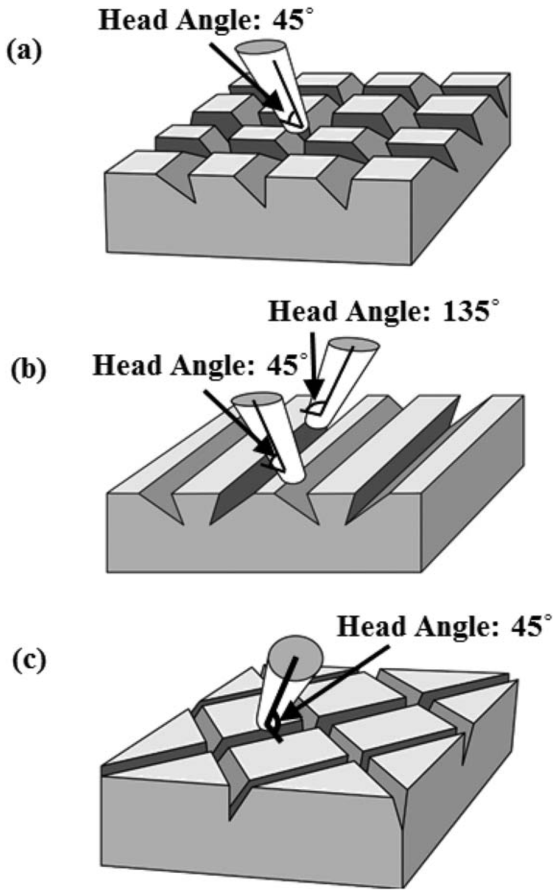

FIG. 3. Schematic drawings of laser machining pattern on the metal surface. (a) Right angle cross path (laser head angle: 45°), (b) Parallel line path (laser head angle: 45° and 135°), (c) Diagonal cross path (laser head angle: 45°).

metal surface, thereby forming an engraved metal surface. The particles used for electroplating should be non-electrolytic to prevent them from aggregating, and their specific gravity should be higher than that of the solution since they should remain submerged in the solution. For the metal surface plating, we used the following particles: glass beads, ceramic beads, artificial diamonds, and aluminum oxide. The plating height was set to 1/2 the level of particle size.

Plating using glass beads. A glass bead has a globular shape and smooth surface. The surface of the metal specimen was plated using glass beads with three sizes of diameters: 60–90, 100–125, and 125–150 μm.

Plating using ceramic beads. A ceramic bead has a spherical shape similar to that of the glass bead but it has a matt surface, which is different from the glassy texture of the glass bead. The surface of the metal specimen was plated using ceramic beads with three sizes of diameters: 30–60, 100–125, and 125–150.

Plating using artificial diamonds. The shape of an artificial diamond contains overlapping prismatic and trapezoidal columns that have smooth surfaces but irregular shapes. It has a structure that becomes narrower at the top and bottom. A metal specimen was fabricated using artificial diamonds with three sizes of diameters: 45, 106, and 150 μm.

Plating Using Aluminum Oxide. Aluminum oxide is an irregularly shaped whetstone powder used in grinding. The shape of aluminum oxide is highly irregular, rough, and sharp. In this study, the surface of the metal specimen was plated using particles of aluminum oxide with three sizes of diameters: 63–90, 125–150, and 180–212.

Figure 4 shows the metal surfaces after plating with glass beads, ceramic beads, artificial diamonds, and aluminum oxide

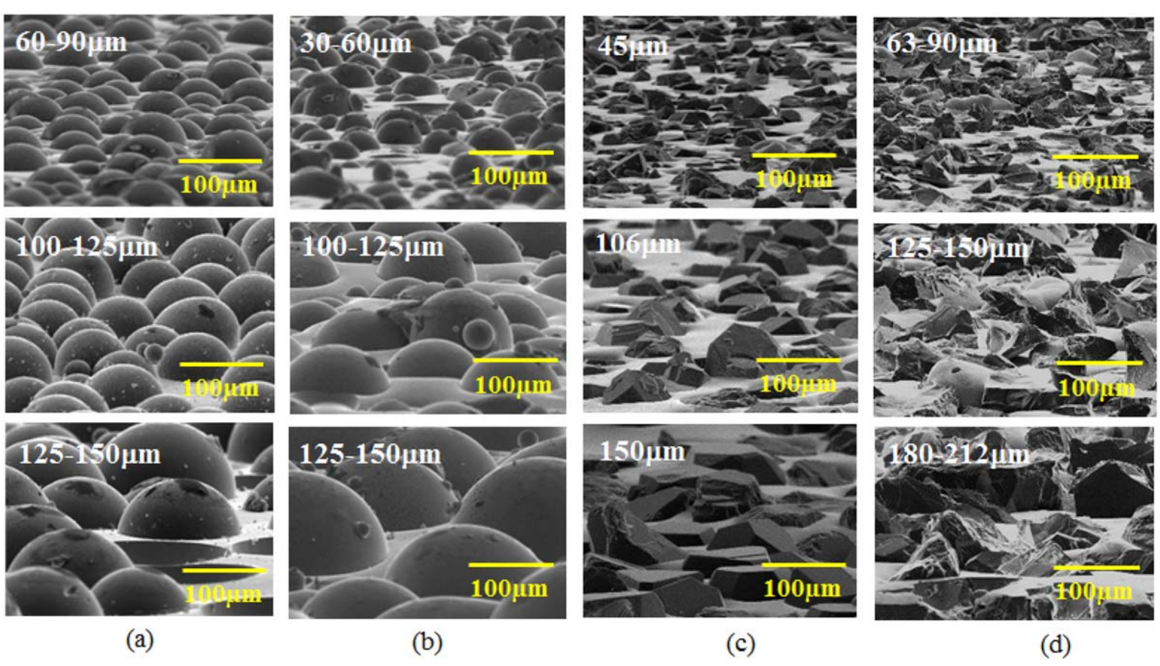

FIG. 4. SEM photo of metal specimen surface after plating using particles (×500 View). (a) Glass beads, (b) Ceramic beads, (c) Artificial diamond, (d) Aluminum oxide.

observed using a scanning electron microscope (SEM). A SEM photo verified that the plating height was up to 1/2 the height of the particles.

Metal Insert Molding

A lab-shear test specimen was manufactured for adhesive strength testing where metal and plastic were bonded via insert molding using metal specimens fabricated according to each of the surface treatment conditions. The mold for the metal insert molding was designed to obtain two specimens with one injection molding operation. The molding conditions for the metal insert molding were as follows. The filling phase was set at four levels of speed, 100, 70, 150, and 180 mm/s, and the packing phase was set at three stages, 60, 150, and 80 MPa for 2, 6, and 2 s, respectively. The screw position of the V/P switchover was 10 mm. An 80-ton injection molding machine (TE110, Woojin Plaimm) was used. The injection temperature was set to 260°C; the mold temperature at the fixed side was set to 80°C by installing a cartridge heater while that at the moving side room temperature was maintained.

Measurement of Adhesive Strength

Lab-shear tests were conducted to evaluate the adhesive strengths of specimens where metal and plastic were adhered using insert molding. The tensile tester for the lab-shear test used in this study was EZ20 (AMETEK Sensors, Test and Calibration). The extension rate was set at 1 mm/min and the maximum extension force was measured while a force was applied until the bonded surfaces separated. The adhesive strength was calculated by dividing the measured maximum extension force by the bonded area between the metal and ABS.

RESULTS AND DISCUSSION

Adhesive Strength between the Laser-Machined Metal Sheet and ABS

The results of lab-shear testing on the specimens manufactured by insert molding after laser surface treatment are presented in Table 2. A relatively high adhesive strength was achieved in all the machining paths with processing laser head angles of 45° or 135°. However, no adhesion was observed between the metal and plastic with a processing laser head angle of 90°. In particular, the highest adhesive strength was revealed when the metal specimen was processed along the right angle cross path at a laser head angle of 45° followed by processing along the diagonal cross path at a laser head angle of 45°. The lowest adhesive strength was revealed in specimens processed along the parallel line path using an alternate laser head angle of 45° and 135°. Figure 5a shows a metal surface processed along the right angle cross path at a laser head angle of 90° and Fig. 5b shows a metal surface processed along the right angle cross path at a laser head angle of 45°. The laser-processed impression on the metal surface in Fig. 5a was deep and clear but no undercut shape was seen. In contrast, the metal surface in Fig. 5b had an undercut space which was obliquely dented inside. Adhesive strength was improved significantly by making an undercut shape at the surface by changing the laser head angle under the same conditions. The above result showed that whether an undercut shape was present or not significantly influenced the adhesive strength between metal and plastic. Figure 6 shows a metal surface processed along the parallel line path alternately at laser head angles of 45° and 135°. The metal surface processed along the right angle cross and diagonal cross paths held the plastic in two directions, whereas the metal surface processed along the parallel line path held the plastic only in one direction. As a result, lower adhesive strength was revealed under conditions processed along the parallel line path than under other path conditions.

TABLE 2. Lab-shear test results for laser-machined metal sheet.

Machining path	Laser head angle	Resin	Adhesive strength [kPa]
Right angle cross	45°	ABS+GF	1,471.91
	90°	(30 wt%)	NA
Parallel line	45°, 135°		701.86
Diagonal cross	45°		936.46

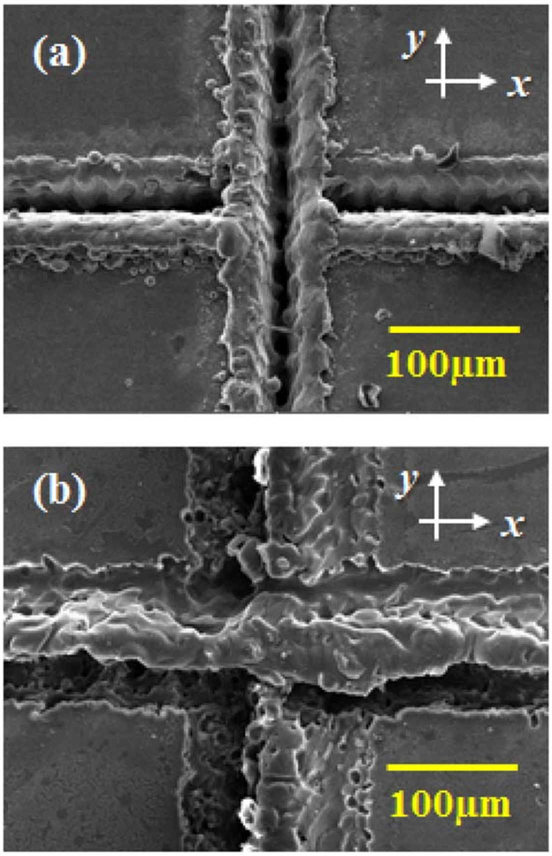

FIG. 5. SEM photo of the laser-machined metal surface for a right angle cross (×500 View). (a) A 90° laser head angle, (b) A 45° laser head angle.

The metal surface that was processed with a laser head angle of 90° exhibited the lowest adhesive strength even when the machine path was at a right angle cross. Specimens processed along the parallel line path to the tensile direction with laser head angles of 45° and 135° had some degree of adhesive strength. This phenomenon revealed that the laser head angle is a primary factor for adhesive strength between plastics and laser-machined metal surfaces because the inclined laser head angle provided an undercut space on the metal surface.

 DOI 10.1002/pen

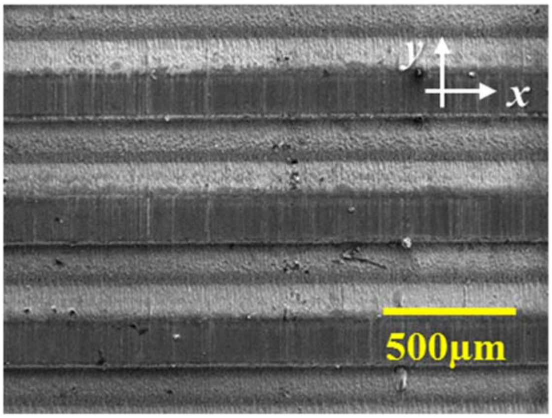

FIG. 6. SEM photo of laser-machined metal surface for a parallel line (×100 view).

Adhesive Strength Between Plated Metal Sheet and ABS

Glass Bead-Plated Metal Sheet. Table 3 presents lab-shear testing results on the specimens fabricated by insert molding after plating on the metal surface using glass beads. The metal and plastic did not adhere under any conditions, regardless of the particle size. Figure 7 shows the surfaces separated after lab-shear testing on the specimens with glass beads of 60–90 μm as seen in the SEM image. Since most particles remained on the metal side, the plastic seemed to escape the metal surface easily. The glass bead impression on the plastic surface was seen vividly as plastic was easily separated (Fig. 7b). Although metal and plastic contacted completely, the metal surface did not hold the plastic securely, which was the reason for insufficient adhesive strength.

Ceramic Bead-Plated Metal Sheet. Table 4 presents lab-shear testing results on the specimens fabricated with insert molding after plating on the metal surface using ceramic beads. The metal and plastic did not adhere regardless of particle size. Figure 8 shows the surfaces separated after lab-shear testing on the specimens using ceramic beads of 30–60 μm as seen in the SEM image. As shown in the figure, most particles remained on the metal side. Impressions where ceramic beads escaped were clearly seen on the plastic surface. This result was obtained because the plastic was easily separated from the metal surface since the metal surface could not hold the plastic securely—the same behavior as that with glass beads—resulting in insufficient adhesive strength.

Artificial Diamond-Plated Metal Sheet. Table 5 presents lab-shear testing results on the specimens fabricated by insert molding after plating on the metal surface using artificial diamonds. The adhesive strength increased as the particle size increased. A specimen using 150 μm artificial diamond particles—which was the largest particle size among the tested specimens—had much stronger adhesive strength than those of specimens processed by laser. Furthermore, adhesive strength improved by two to three times with a metal surface using existing engraving methods, such as etching. A limitation of the adhesive area that can be enlarged by existing engraving surface treatment was overcome using the embossing method, which attached particles to the metal surface. The irregular shape of artificial diamonds enlarged the surface area, and particles adhering to the metal surface formed an undercut space. These factors were deemed to increase the adhesive strength between metal and plastic. The generated undercut space became larger as the particle size used in the plating became larger. Thus, better adhesive strength was obtained as particle size increased. Figure 9 shows the surface separated after lab-shear testing on the specimen using artificial diamond particles of 150 μm according to the SEM image. The surface of the plastic showed that the irregular artificial diamond particles escaped the plastic with difficulty.

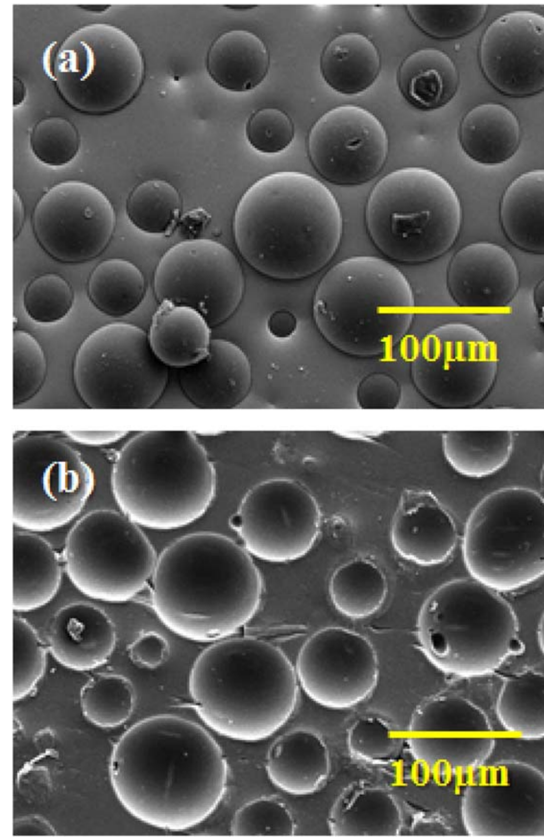

FIG. 7. SEM photo of metal and plastic surfaces after lab-shear test for 60–90-μm glass beads plated metal (×500 view). (a) Metal surface, (b) Plastic surface.

TABLE 3. Lab-shear test results for glass bead-plated metal sheet.

Particle	Resin	Particle size [μm]	Plating height for Particle Size	Adhesive strength [kPa]
Glass beads	ABS + GF (30 wt%)	60–90	1/2	NA
		100–125		NA
		125–150		NA

TABLE 4. Lab-shear test results for ceramic bead-plated metal sheet.

Particle	Resin	Particle size [μm]	Plating height for particle size	Adhesive strength [kPa]
Ceramic beads	ABS + GF (30 wt%)	30–60	1/2	NA
		100–125		NA
		125–150		NA

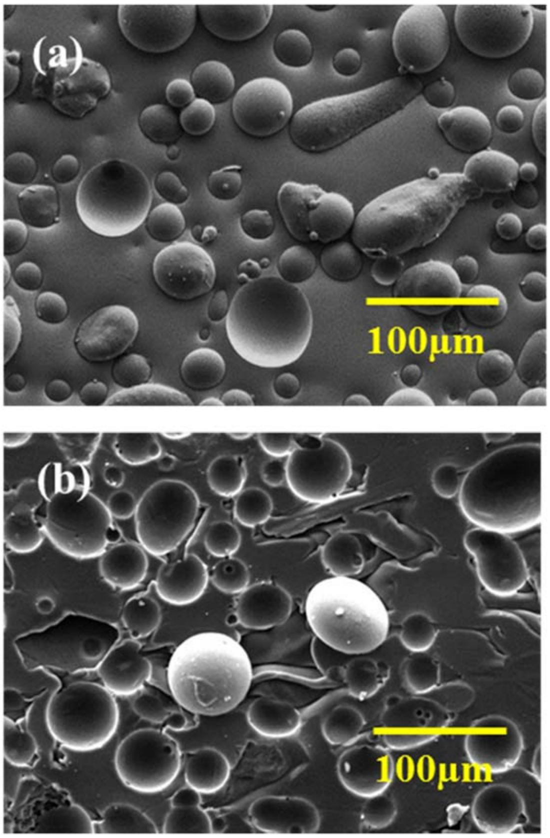

FIG. 8. SEM photo of metal and plastic surfaces after lab-shear test for 30–60-μm ceramic beads plated metal (×500 view). (a) Metal surface, (b) Plastic surface.

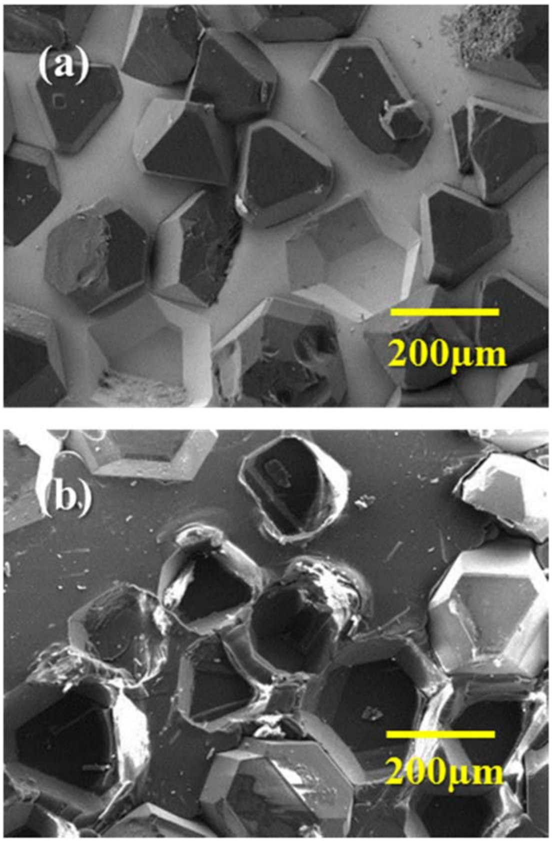

FIG. 9. SEM photo of metal and plastic surfaces after lab-shear test for 150-μm artificial diamonds plated metal (×200 View). (a) Metal surface, (b) Plastic surface.

Aluminum Oxide-Plated Metal Sheet. Table 6 presents lab-shear testing results on the specimens fabricated by insert molding after plating on the metal surface using aluminum oxide. Overall, stronger adhesive strength was revealed than when artificial diamond particles were used. The adhesive strength increased with the particle size of aluminum oxide. When aluminum oxide was used, the adhesive area increased by means of its rough surface, and the effect of undercut space generation seemed significant. The shape of aluminum oxide particles is less regular than that of artificial diamond particles. Thus, the aluminum oxide particles generated various undercut spaces in multiple directions on the metal surface, which provided mechanical interlocking, thereby holding the plastic effectively. Figure 10 shows the surface separated after lab-shear testing on the specimen using aluminum oxide plating (180–212 μm), as shown in the SEM image. Broken GF was observed on the surface of the plastic. The rough and sharp shape of aluminum oxide seemed to break the protruding GF at the surface of the

TABLE 5. Lab-shear test results for artificial diamond-plated metal sheet.

Particle	Resin	Particle size [μm]	Plating height for particle size	Adhesive strength [kPa]			
				1	2	3	Average
Artificial diamonds	ABS + GF (30 wt%)	45	1/2	NA	NA	NA	NA
		106		68.23	217.03	166.57	150.61
		150		2,045.62	1,905.88	2,035.46	1,995.65

 DOI 10.1002/pen

TABLE 6. Lab-shear test results for aluminum oxide-plated metal sheet.

Particle	Resin	Particle size [μm]	Plating height for particle size	Adhesive strength [kPa]			
				1	2	3	Average
Aluminum oxide	ABS + GF (30 wt%)	63–90	1/2	177.44	178.61	167.11	174.39
		125–150		943.72	929.85	975.03	949.53
		180–212		2,291.53	2,271.53	2,344.61	2,302.55

plastic. The GF contained in the ABS reduced the difference in shrinkage ratios between the metal and ABS, thereby decreasing the shear stress at the interface, resulting in improved adhesive strength. However, if the GFs inhibit close contact between the metal surface and plastic due to protruding GFs on the plastic surface, they may instead cause a side effect that degrades the adhesive strength between the metal and plastic [24]. Since the surface of the aluminum oxide was rough, the rough surface broke the GF, which inhibited contact between the metal surface and the ABS to make the contact more secure, thereby obtaining superior adhesive strength.

CONCLUSIONS

This study investigated improvements in adhesive strength between the metal and GF-filled ABS. To do this, the surface of metal specimens was processed with various conditions using laser processing (engraving method) and plating (embossed method). Metal and ABS were bonded via insert molding using the processed metal specimens, and the adhesive strength was evaluated according to the surface treatment condition on the metal.

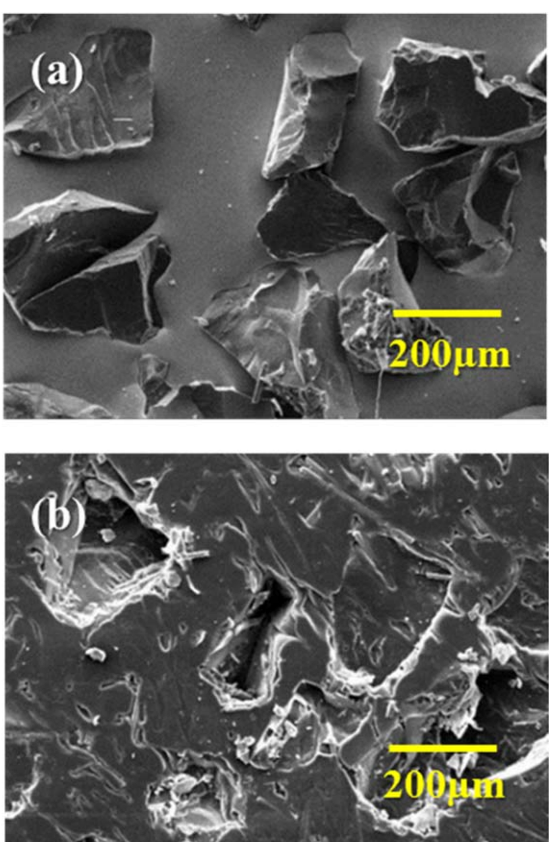

FIG. 10. SEM photo of metal and plastic surfaces after lab-shear test for 180–212 μm aluminum oxide (×200 view). (a) Metal surface, (b) Plastic surface.

The test results on adhesive strength between GF-filled ABS and metal with a surface that was processed with a laser showed that the best adhesive strength was obtained when an undercut shape was generated at the surface obliquely at a laser head angle of 45° or 135°. This was because an undercut shape was formed on the metal surface according to the laser head angle of the laser processing machine.

Adhesive strength test results between GF-filled ABS and metal with a surface that was plated using glass beads and ceramic beads showed that metal and plastic did not adhere well, regardless of particle size. The surfaces of these particles were smooth and no undercut spaces were formed on the metal surface.

Adhesive strength test results between the metal and GF-filled ABS with a surface that was plated using artificial diamond and aluminum oxide showed that the adhesive strength increased significantly relative to the existing metal surface treatment method. In particular, when aluminum oxide was used, the adhesive strength was very strong. This was because the irregular shape and rough surface of the aluminum oxide increased the area of contact with the ABS and provided undercut spaces of various shapes at the metal surface.

REFERENCES

1. H.M. Khalid, and M.G. Helander, *Concurrent Engineering*, **14**, 197 (2006).
2. D.A. Norman, *Interactions*, **9**, 36 (2002).
3. S.L. Kim, T.G. Choi, H.S. Cho, M.-Y. Lyu, J. Lim, and S. Lee, *Polymer(Korea)*, **40**, 871 (2016).
4. Carla I. Martins, I. Santos, A. J. Pontes, *International PMI Conference Proceeding*, Vol. **5**, 375 (2012).
5. H.Y. Kim, M.-Y. Lyu, and J.G. Choi, *Trans. Mater. Process.*, **18**, 156 (2009).
6. N.M. Zain, S.H. Ahmad, and E.S. Ali, *Int. J. Adhes. Adhes.*, **55**, 43 (2014).
7. M. Grujicic, V. Sellappan, M.A. Omar, N. Seyr, A. Obieglo, M. Erdmann, and J. Holzleitner, *J. Mater. Process. Technol.*, **197**, 363 (2008).
8. M. Honkanen, M. Hoikkanen, M. Vippola, J. Vuorinen, and T. Lepistö, *J. Adhes. Sci. Technol.*, **23**, 1747 (2009).
9. A. G. Alkins and Y. W. Mai, *Elastic and Plastic Fracuture*, John Wiley & Sons, NY, 289 (1985).

10. K. L. Mittal, Ed. *Progress in Adhesion and Adhesives*, Scrivener Publishing, Hooken, 9 (2015).
11. K.L. Mittal, *Polym. Eng. Sci.*, **17**, 467 (1977).
12. G. Fourche, *Polym. Eng. Sci.*, **35**, 957 (1995).
13. K. Ramani, and B. Moriarty, *Polym. Eng. Sci.*, **38**, 870 (1998).
14. Y. Kim, and S. Kil, *J. Welding Join.*, **34**, 62 (2016).
15. P.K. Ghosh, A. Patel, and K. Kumar, *Polymer*, **87**, 159 (2016).
16. J. Abenojar, A.Q. Barbosa, Y. Ballesteros, J.C. del Real, L.F.M. da Silva, and M.A. Martínez, *Wood Sci. Technol.*, **48**, 207 (2014).
17. F. Habouzit, G. Gévaudan, J. Hamelin, J.-P. Steyer, and N. Bernet, *Bioresource Technol.*, **102**, 4054 (2011).
18. Y. Nakamura, Y. Suzuki, and Y. Watanab, *Thin Solid Films*, **290–291**, 367 (1996).
19. G. Lucchetta, F. Marinello, and P.F. Bariani, *Int. Inst. Prod. Eng. Res.*, **60**, 559 (2011).
20. A.F. Harris, and A. Beevers, *Int. J. Adhes. Adhes.*, **19**, 445 (1999).
21. B. Bhushan, and M. Nosonovsky, *Philos. Trans. Ser. A Math., Phys. Eng. Sci.*, **368**, 4713 (2010).
22. R. Matsuzaki, N. Tsukamoto, and J. Taniguchi, *Int. J. Adhes. Adhes.*, **68**, 124 (2016).
23. J.W. Dini, and H.R. Johnson, *Surf. Technol.*, **5**, 405 (1977).
24. S.L. Kim, M.-Y. Lyu, and S.W. Jang, *Polymer(Korea)*, **41**, 727 (2017).